

# Efficient Measurement of the Bi-photon Spatial Mode Entanglement with Stimulated Emission Tomography

Yang Xu

*Department of Physics and Astronomy, University of Rochester, Rochester, New York 14627, USA*<sup>\*</sup>

Saumya Choudhary

*The Institute of Optics, University of Rochester, Rochester, New York 14627, USA*

Robert W. Boyd

*Department of Physics and Astronomy, University of Rochester, Rochester, New York 14627, USA*

*Department of Physics, University of Ottawa, Ottawa, Ontario K1N 6N5, Canada*

*The Institute of Optics, University of Rochester, Rochester, New York 14627, USA*

The technique of stimulated emission tomography (SET) provides excellent characterization of SPDC sources of bi-photon states since it increases the average number of photons detected by several orders of magnitude than the traditional coincidence counting method. In a SET experiment, the signal caused by the vacuum fluctuation in SPDC is replaced by a more intense prepared seed with the same mode properties, resulting in an amplification of the corresponding idler. Based on this idea, our experiment uses the difference frequency generation (DFG), a purely classical second-order nonlinear process, to measure the orbital angular momentum (OAM) spectrum of an entangled photon pair produced by a Type-II SPDC crystal. We inject the seed beam at 780 nm with different Laguerre-Gaussian modes together with a pump beam at 405 nm into a Type-II BBO crystal and measure the Laguerre-Gaussian mode distribution of the idler at 842 nm. We observe a strong idler production and good agreement with the theoretical prediction of the OAM spectrum. We expect that this experiment paves the way for the efficient measurement of bi-photon wavefunctions produced by ultra-thin SPDC sources and also the characterization of high-dimensional entangled photon pairs produced in SPDC.

*Introduction.*—Entangled photon pairs have become an essential part of many quantum imaging [1–3] and quantum information experiments[4, 5]. Recent studies have shown that high-dimensional entanglement has unique advantages in developing secure quantum communication protocols[6], demonstrating the violation of Bell’s inequality[7, 8], and substantiating the EPR paradox[9]. It was shown that the orbital angular momentum (OAM) of photons is a convenient and natural choice of a high-dimensional basis[10]. Therefore, the OAM-entangled photon pairs have become a strong candidate for the implementation of high-dimensional quantum information protocols[11, 12]. As a result, there has been a plethora of research efforts, both theoretically[13–15] and experimentally[16, 17], for the accurate and efficient characterization of high-dimensional OAM entanglement in spontaneous parametric down-conversion (SPDC).

In a more general sense, the spatial modes of signal and idler photons produced by SPDC are entangled. The spatial structure of the down-converted photons produced in SPDC can be written in terms of a mode decomposition of their two-photon wave function in a complete set of spatial mode basis. Usually, the spatial modes of photons are decomposed into Laguerre-Gaussian (LG) modes,  $LG_p^l$  where  $l$  represents the orbital angular momentum carried by the photon,  $l\hbar$ , and  $p$  corresponds to

the radial mode. Measuring the probability amplitude of each basis mode is the core task in the characterization of high-dimensional spatial mode entanglement. There have been extensive research efforts[16, 18–20] on the measurement of the two-photon entanglement in OAM modes, also known as the spiral bandwidth. In these works, the use of image-rotating interferometers[16, 19] and the traditional coincidence counting method[21] are the two common ways to measure the spiral bandwidth. Because of the low efficiency of SPDC processes, these two methods require painstaking alignment, an environment free from perturbations, and long data acquisition time. Furthermore, the SPDC experiments so far are only capable of measuring the OAM ( $l$ ) correlation of entangled photon pairs where the contributions from individual radial modes ( $p$ ) are summed up[20].

However, the radial mode ( $p$ ) is also an important quantum number describing the radial-momentum-like property of Laguerre-Gaussian modes. The entanglement in radial modes offers a larger number of qubits that can be used in quantum communication[22]. In addition, the use of radial modes is essential in entanglement control with topological knots of phase and polarization singularities[23]. These knot structures can be generated by specific superposition of radial and orbital angular momentum modes[24]. It has been shown by experiments that the knot structures are robust against turbulence[25]. This feature may become useful in the propagation of entanglement in turbulent media. A full modal analysis, including the radial modes, of the two-

<sup>\*</sup> yxu100@ur.rochester.edu

photon spatial mode entanglement produced by SPDC has been worked out in theory[13]. In principle, the theoretical results can be verified by converting to the fundamental mode of single-mode fibers and measuring the coincidence rate, but the measurement in a real-world laboratory setting is experimentally challenging due to the extremely low photon pair production rate if they are projected onto a specific spatial mode.

Fortunately, recent works[26] have shown that one can study the stimulated parametric down-conversion to extract information about the bi-photon state produced in its spontaneous counterparts. This technique is known as stimulated emission tomography (SET). By exploiting the link between spontaneous and stimulated processes, SET offers an efficient way to measure the bi-photon state with a signal-to-noise ratio several orders of magnitude larger than the traditional quantum state tomography method[27, 28]. This large enhancement in signal-to-noise ratio allows the use of classical detectors in the measurement of the joint spectral density of entangled photon pairs[29, 30]. In this letter, we apply the SET theory and demonstrate a new way to efficiently measure the entanglement of Laguerre-Gaussian (LG) modes of the photon pair produced in SPDC pumped by a Gaussian beam. By changing the LG modes of the input seed beam so that the output signal ranges through all the possible LG modes that a spontaneously generated signal might have in the absence of the seed, and measuring the relative magnitude of the amplified idler output in the presence of the seed, we can reconstruct the bi-photon LG mode spectrum of the photon pair produced in the absence of the seed.

*Theory.*—Consider a typical SPDC setup that consists of a continuous Gaussian pump beam with frequency  $\omega_p$  propagating along the  $z$  direction incident on a thin nonlinear crystal of length  $L$ . The output bi-photon state after the nonlinear crystal in the momentum domain is given by[31]

$$|\psi\rangle = \iint d\mathbf{k}_s d\mathbf{k}_i \Phi(\mathbf{k}_s, \mathbf{k}_i) \hat{a}_s^\dagger(\mathbf{k}_s) \hat{a}_i^\dagger(\mathbf{k}_i) |0\rangle \quad (1)$$

where  $\Phi(\mathbf{k}_s, \mathbf{k}_i)$  is the bi-photon wave function describing the pump and the phase matching conditions,  $\hat{a}_s^\dagger(\mathbf{k}_s)$ ,  $\hat{a}_i^\dagger(\mathbf{k}_i)$  are creation operators for the signal and idler modes with wave vectors  $\mathbf{k}_s$  and  $\mathbf{k}_i$ . The subscripts  $p, s, i$  refers to the pump, signal and idler respectively. To characterize the spatial mode entanglement of an SPDC source, we need to calculate the coincidence probability  $P_{p_s, p_i}^{l_s, l_i} = |C_{p_s, p_i}^{l_s, l_i}|^2$  where the coincidence amplitude  $C_{p_s, p_i}^{l_s, l_i}$  is given by the integral

$$C_{p_s, p_i}^{l_s, l_i} = \iint d\mathbf{k}_s d\mathbf{k}_i \Phi(\mathbf{k}_s, \mathbf{k}_i) [LG_{p_s}^{l_s}(\mathbf{k}_s)]^* [LG_{p_i}^{l_i}(\mathbf{k}_i)]^* \quad (2)$$

The coincidence probability  $P_{p_s, p_i}^{l_s, l_i}$  corresponds to the probability for finding a signal in an LG mode characterized by  $LG_{p_s}^{l_s}$  and an idler photon in the mode  $LG_{p_i}^{l_i}$ .

Assuming a monochromatic Gaussian pump and a thin crystal, the coincidence amplitude becomes [13, 32]:

$$C_{p_s, p_i}^{l, -l} \propto A_{p_s, p_i}^{|l|} \frac{(1 - \gamma_s^2 + \gamma_i^2)^{p_s} (1 + \gamma_s^2 - \gamma_i^2)^{p_i} (-2\gamma_s\gamma_i)^{|l|}}{(1 + \gamma_s^2 + \gamma_i^2)^{p_s + p_i + |l|}} {}_2F_1 \left( -p_i, -p_s; -p_i - p_s - |l|; \frac{1 - (\gamma_s^2 + \gamma_i^2)^2}{1 - (\gamma_s^2 - \gamma_i^2)^2} \right) \quad (3)$$

where  $A_{p_s, p_i}^{|l|} = (p_s + p_i + |l|)!/\sqrt{p_s!p_i!(p_s + |l|)!(p_i + |l|)!}$ ,  ${}_2F_1$  is the Gaussian hypergeometric function,  $\gamma_i = w_p/w_i$  and  $\gamma_s = w_p/w_s$  are the inverses of the normalized signal and idler beam waist measured with respect to the pump beam. We noticed that the orbital angular momentum conservation,  $l_s = -l_i = l$ , must be satisfied as a result of the integral in Eq. 2.

Due to the symmetry between the signal and the idler, we have  $w_p = w_i$ , so  $\gamma_i = \gamma_s = \gamma$ . For computational and experimental simplicity, we set  $p_s = p_i = 0$  in our experiment. Thus, the coincidence probability we want to measure in our experiment further simplifies to

$$P_{0,0}^{l, -l} = |C_{0,0}^{l, -l}|^2 \propto \left( \frac{2\gamma^2}{1 + 2\gamma^2} \right)^{2|l|} \quad (4)$$

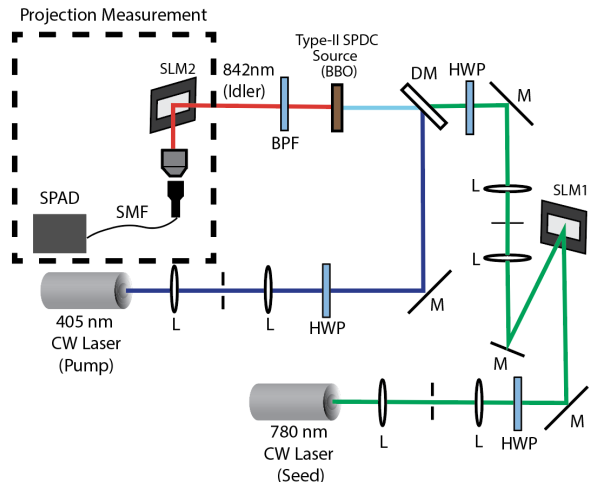


FIG. 1. Schematic of the experimental setup. L: lens; HWP: half-wave plate; BPF: band-pass filter; SMF: single-mode fiber; DM: dichroic mirror. A Type-II BBO crystal is pumped by a 405 nm CW laser beam with a Gaussian spatial profile (drawn in blue). The seed OAM is generated by a hologram printed on SLM. The seed prepared in the first diffraction order is picked out by the pinhole and injected into the Type-II BBO crystal together with the Gaussian pump beam. The output idler is passed to the OAM projection measurement setup where the intensity of the projected beam is measured to construct the OAM spectrum

*Experiment.*—Fig. 1 shows the SET setup used to measure the LG mode spectrum with SET. We pump

a 10-mm-long Type-II beta barium borate (BBO) crystal with a horizontally polarized, 30 mW, c.w. 405 nm collimated Gaussian beam ( $LG_0^0$ ). The pump beam is produced by a laser diode and has a diameter of 2 mm. The 780-nm seed beam carrying a fixed OAM charge,  $l_s$ , is picked out at the first diffraction order by passing a collimated c.w. Gaussian beam at 780 nm through an OAM-generating hologram printed on SLM 1 (Meadowlark E-series 1920  $\times$  1200 SLM). The prepared seed beam in a Laguerre-Gaussian mode  $LG_0^{l_s}$  is then injected into the BBO nonlinear crystal together with the Gaussian pump beam at 405 nm. Both the pump and the seed beam were spectrally filtered with a narrowband filter (10 nm) centered at 405 nm and 780 nm respectively. A half-wave plate was placed after each narrowband spectral filter to control the polarization of the pump and the signal beam so that the phase-matching condition of the difference frequency generation is satisfied. By aligning the seed beam with the SPDC signal of the same polarization, the seed beam is amplified by a stimulated parametric down-conversion process and the idler beam with an opposite OAM number  $l_i = -l_s$  is generated. The down-converted idler beam is selected out by a narrowband (10 nm) filter centered at 840 nm. A second SLM (Santec SLM-200) is used to project the filtered idler onto different OAM eigenmodes[33, 34]. The hologram we put on SLM2 converts the  $LG_0^{l_i}$  into a Gaussian beam. The converted Gaussian beam is then coupled to a single-mode fiber (SMF). A single photon avalanche diode (SPAD) is used to measure the total number of photons coupled into the SMF.

*Result.*—We first verify the validity of the thin-crystal approximation in our experiment. The 405-nm Gaussian pump beam we use in our experiment has a waist of 2.7 mm. The thin-crystal approximation for this pump beam is valid when  $L \ll z_R$  where  $L$  is the length of the crystal and  $z_R$  is the Rayleigh range of the pump beam. This condition is equivalent to  $w_p/\sqrt{\lambda_p L} \gg 1$  [35]. In our experiment, the length of our Type-I BBO crystal is  $L = 2.0$  mm, so the quantity  $w_p/\sqrt{\lambda_p L} \approx 94.8 \gg 1$ . Thus, the thin-crystal approximation is suitable for our experiment.

We measure the number of photons collected by the SPAD over ten 5-second time windows for different seed OAM modes ranging from  $l = -6$  to  $l = 6$ . To calibrate the measurement, we block all beams and collect the dark counts collected by the SPAD to characterize the background effect over twenty 5-second time intervals. The mean value and the fluctuation of dark counts will be subtracted in our data analysis.

In Fig. 2, we show the measurements of the two-photon joint spectral amplitude (JSA) in OAM space. The two-dimensional (2D) JSA is measured in the following way. First, we fix the static OAM generating hologram on SLM1 so that the seed beam has a pre-determined spatial profile  $LG_0^{l_s}$ . The idler produced in the parametric down-conversion is then passed to another hologram that generates  $LG_0^{l_i}$  on SLM2. This hologram

on SLM2 converts the  $LG_0^{l_i}$  component in the idler beam into a Gaussian profile in the first diffraction order. Finally, we scan through multiple  $l_i$  values by altering the OAM-generating hologram on SLM2 and record the corresponding number of photons coupled to the SPAD for each  $l_i$ . We switch to a different seed mode and repeat the procedure above to measure the full 2D JSA matrix. We notice that only the blocks where  $l_i = l_s$  is satisfied are significant given a Gaussian pump beam ( $LG_0^0$ ) at 405 nm. The measured two-photon JSA agrees with theoretical calculations and thus confirms the conservation of OAM in collinear SPDC processes.

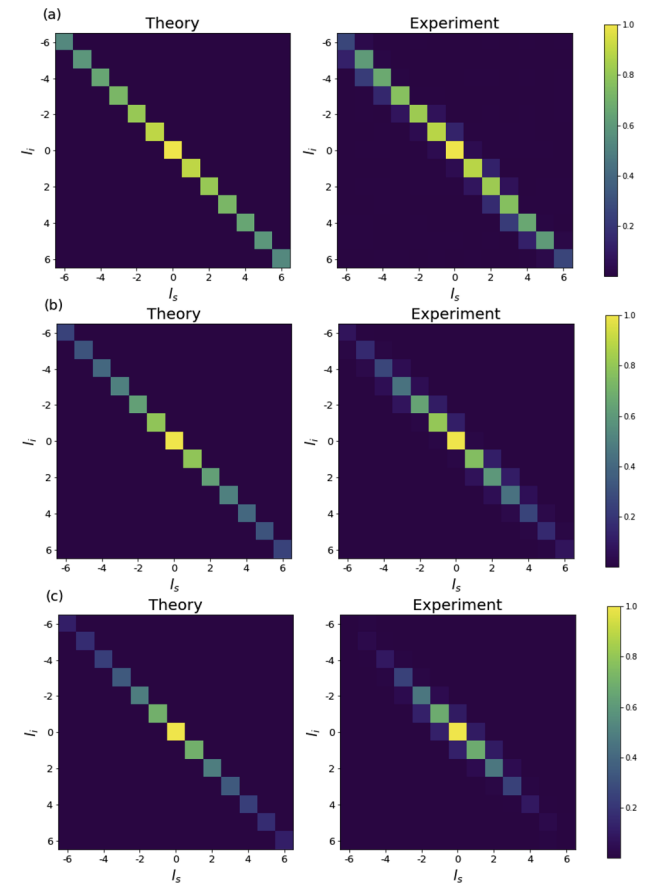


FIG. 2. Two-photon JSA by SET compared to theoretical predictions. The hologram on SLM2 iterates through OAM modes along each column where the seed OAM is held fixed. The magnitude of JSA is then measured in the number of photons coupled into the SMF. The width of the pump is kept constant at 2 mm. (a) OAM spectrum at  $w_i = w_s = 0.72$  mm (b) OAM spectrum at  $w_i = w_s = 1.08$  mm (c) OAM spectrum at  $w_i = w_s = 1.35$  mm.

In Fig. 3, we plot the LG mode probability distribution for two different seed waists using our SET experiment and compare them to theoretical calculations. By comparing the two spectra at two different seed waists, we notice an increase in the spectrum width as the seed beam waist decreases. This effect will be discussed in

detail later in this section. In Fig. 3(a) where the seed width is larger ( $\gamma_s = \gamma_i = 2.03$ ), one may observe a noticeable discrepancy between theoretical predictions and the measured data for higher OAM modes. This is due to the decrease in the coupling efficiency of the fiber coupler connected to the SMF. The projection phase mask on SLM2 converts the beam with a higher OAM number into a wider Gaussian profile. Thus, for each OAM projection phase mask on SLM2, the fiber coupling efficiency varies slightly. This deviation from the optimal fiber coupling becomes obvious for smaller  $\gamma_s$  (larger  $w_s$ ) since the width of the converted Gaussian starts to exceed the capability of the objective we use in our fiber coupling system. Fortunately, this problem can be easily solved in principle by using an objective with a suitable effective focal length for the projection measurement of each OAM mode.

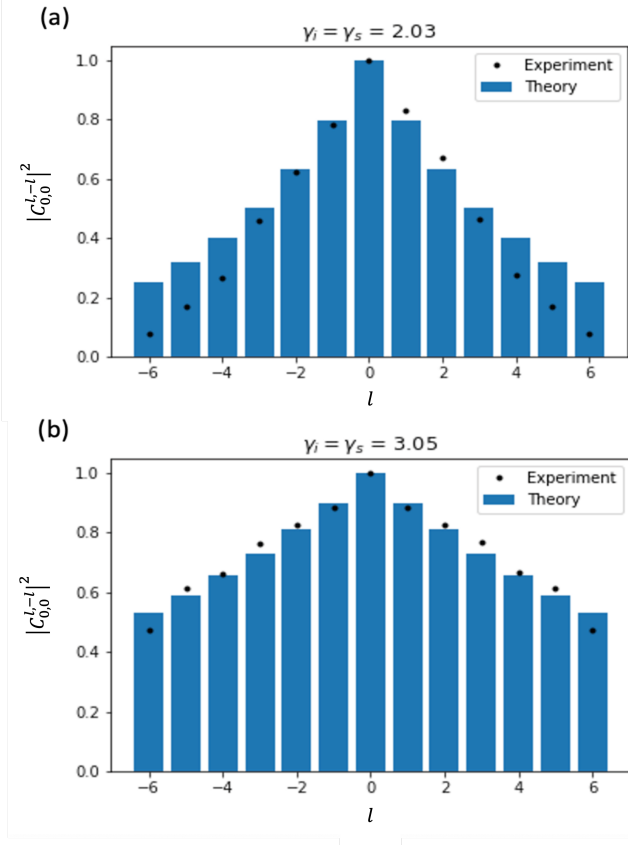


FIG. 3. OAM spectrum measured by SET compared to theoretical predictions. The beam width of the output idler is the same as the seed width due to the nature of a stimulated process. The spread in the OAM spectrum is clearly observed as the normalized seed and idler beam widths increase suggesting a larger spatial overlap between the seed and the pump. (a) OAM spectrum at  $\gamma_i = \gamma_s = 2.03$  (b) OAM spectrum at  $\gamma_i = \gamma_s = 3.05$

Now, we study the dependence of the OAM spectrum on seed and pump waists. As shown in Eq. 2, the weight of each LG mode should depend on the ratio between

the pump and the signal/idler widths,  $\gamma_{s,i} = w_p/w_{s,i}$ . In stimulated parametric down-conversions, the relation  $\gamma_s = \gamma_i$  is automatically satisfied, so the probability amplitude of each OAM mode only depends on the normalized beam waist  $\gamma = \gamma_s = \gamma_i$ . To better understand the OAM spectral broadening dependent on the beam waist in a quantitative way, we plot the normalized coincidence probability of the photon pair production,  $|C_{0,0}^{l,-l}|^2$ , as a function of the pump-normalized beam waist,  $\gamma$ , for three different values of  $l_i$  and  $l_s$  with  $l_i + l_s = 0$  in Fig. 4. We notice an increase in the width of the spectrum as the waists of the signal and idler decrease ( $\gamma = \gamma_i = \gamma_s$  increases). This broadening in spectral width is due to the fact that a smaller seed beam waist allows higher OAM modes to have spatial overlap with a fixed pump beam. This results in a higher numerical value of the overlap integral between the two electric field's spatial profiles.

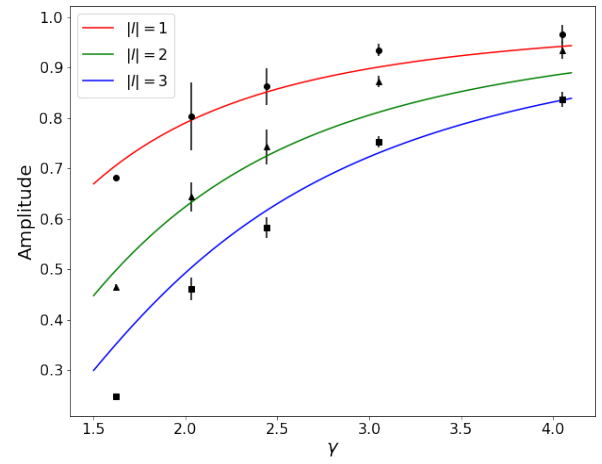


FIG. 4. Dependence of the OAM spectral amplitude on the normalized seed beam waist for  $l_s = -l_i = 1, 2, 3$ .  $\gamma = \gamma_s = \gamma_i = w_p/w_{s,i}$ . The plot shows that the spatial mode spectral amplitude decreases for higher OAM numbers and for larger signal/idler beam waists.

*Discussion.*—In the sections above, we proposed and demonstrated an efficient method to measure the high-dimensional entanglement of photon pairs produced by various SPDC processes. In order to show the great efficiency improvement with our SET method, we examine the SPDC process where the Gaussian pump is down-converted into a fundamental Gaussian signal and idler  $(p_p, l_p) = (p_s, l_s) = (p_i, l_i) = (0, 0)$  as a benchmark case. We fix our pump power at 30 mW. Then we compare the coincidence detection rate measured by the traditional coincidence counting method and the idler photon production rate measured by our SET method. In the coincidence counting setup, the signal and idler are coupled to single-mode fibers, and the coincidence detection rate is measured by single photon detectors

and a coincidence-counting circuit with a time window of  $\sim 13$  ns. Using this method, we measure a coincidence rate of  $\sim 200$  s $^{-1}$ . In comparison, we measure a photon detection rate of  $\sim 65,000$  photons per second with a Gaussian seed beam of  $\sim 9$  mW using our SET technique. This orders-of-magnitude improvement suggests that our experiment based on SET offers a time-saving method to fully characterize the spontaneous nonlinear responses of ultra-thin bulk crystals or novel nonlinear metasurfaces [36] because the intensity of the nonlinear response depends on the propagation length of the beam inside the material. Another main advantage of our experimental scheme is our ability to efficiently measure the full modal structure of the entangled photon pairs produced by SPDC, including both radial and angular parts of Laguerre-Gaussian modes. Current methods based on interferometry[20, 37, 38] or coincidence-counting[39] only measure the OAM spectrum of the down-converted photon pair where the contribution from different radial modes are summed up as long as they share the same angular mode. A direct projection measurement of the spatial mode on the down-converted photon pairs is technically challenging due to the extremely low pair produc-

tion rate. Our method can be applied to directly measure the full two-photon spatial mode spectrum, including both angular and radial modes, with modest modification. To achieve this, we can simply replace the projection measurement unit in our experiment setup with the recently developed radial mode sorters [40] or the latest multiplane light conversion method[41] that can sort the spatial mode of the incident beam in an arbitrary set of spatial mode basis.

*Conclusion.*—In conclusion, we report the first proof-of-principle experiment to measure the full spatial mode spectral amplitude of entangled photon pairs in high-dimensional space produced by an SPDC source with an efficient classical method. We measure the OAM spectral amplitude for the lowest radial modes ( $p_i = p_s = 0$ ) and study its dependence on beam waist in a complete set of Laguerre-Gaussian spatial basis ( $LG_l^p$ ). We proved that our method is also efficient and robust to measure the joint spectral amplitude for arbitrary signal and idler spatial modes produced in SPDC. Our experimental demonstration with the SET technique paves the way for the possible full characterization of many weak down-conversion sources such as novel nonlinear metasurfaces[36].

- 
- [1] R. S. Bennink, S. J. Bentley, R. W. Boyd, and J. C. Howell, Quantum and classical coincidence imaging, *Phys. Rev. Lett.* **92**, 033601 (2004).
- [2] A. N. Black, E. Giese, B. Braverman, N. Zollo, S. M. Barnett, and R. W. Boyd, Quantum nonlocal aberration cancellation, *Phys. Rev. Lett.* **123**, 143603 (2019).
- [3] M. I. Kolobov, *Quantum imaging* (Springer Science & Business Media, 2007).
- [4] M. A. Nielsen and I. L. Chuang, *Quantum computation and quantum information* (Cambridge university press, 2010).
- [5] M. Murao, M. B. Plenio, and V. Vedral, Quantum-information distribution via entanglement, *Physical Review A* **61**, 032311 (2000).
- [6] V. Karimipour, A. Bahraminasab, and S. Bagherinezhad, Quantum key distribution for d-level systems with generalized bell states, *Physical Review A* **65**, 052331 (2002).
- [7] B. Jack, A. Yao, J. Leach, J. Romero, S. Franke-Arnold, D. Ireland, S. Barnett, and M. Padgett, Entanglement of arbitrary superpositions of modes within two-dimensional orbital angular momentum state spaces, *Physical Review A* **81**, 043844 (2010).
- [8] A. Aiello, S. Oemrawsingh, E. Eliel, and J. Woerdman, Nonlocality of high-dimensional two-photon orbital angular momentum states, *Physical Review A* **72**, 052114 (2005).
- [9] J. Leach, B. Jack, J. Romero, A. K. Jha, A. M. Yao, S. Franke-Arnold, D. G. Ireland, R. W. Boyd, S. M. Barnett, and M. J. Padgett, Quantum correlations in optical angle-orbital angular momentum variables, *Science* **329**, 662 (2010).
- [10] M. Erhard, M. Krenn, and A. Zeilinger, Advances in high-dimensional quantum entanglement, *Nature Reviews Physics* **2**, 365 (2020).
- [11] M. Erhard, R. Fickler, M. Krenn, and A. Zeilinger, Twisted photons: new quantum perspectives in high dimensions, *Light: Science & Applications* **7**, 17146 (2018).
- [12] Y. Ren, C. Liu, K. Pang, J. Zhao, Y. Cao, G. Xie, L. Li, P. Liao, Z. Zhao, M. Tur, *et al.*, Spatially multiplexed orbital-angular-momentum-encoded single photon and classical channels in a free-space optical communication link, *Optics letters* **42**, 4881 (2017).
- [13] F. M. Miatto, A. M. Yao, and S. M. Barnett, Full characterization of the quantum spiral bandwidth of entangled biphotons, *Physical Review A* **83**, 033816 (2011).
- [14] C. I. Osorio, G. Molina-Terriza, and J. P. Torres, Correlations in orbital angular momentum of spatially entangled paired photons generated in parametric down-conversion, *Physical Review A* **77**, 015810 (2008).
- [15] J. Torres, A. Alexandrescu, and L. Torner, Quantum spiral bandwidth of entangled two-photon states, *Physical Review A* **68**, 050301 (2003).
- [16] G. Kulkarni, R. Sahu, O. S. Magaña-Loaiza, R. W. Boyd, and A. K. Jha, Single-shot measurement of the orbital-angular-momentum spectrum of light, *Nature communications* **8**, 1054 (2017).
- [17] L. Beltran, G. Frascella, A. M. Perez, R. Fickler, P. R. Sharapova, M. Manceau, O. V. Tikhonova, R. W. Boyd, G. Leuchs, and M. V. Chekhova, Orbital angular momentum modes of high-gain parametric down-conversion, *Journal of Optics* **19**, 044005 (2017).
- [18] M. Krenn, M. Malik, M. Erhard, and A. Zeilinger, Orbital angular momentum of photons and the entanglement of laguerre-gaussian modes, *Philosophical Transactions of the Royal Society A: Mathematical, Physical and Engineering Sciences* **375**, 20150442 (2017).

- [19] R. F. Offer, D. Stulga, E. Riis, S. Franke-Arnold, and A. S. Arnold, Spiral bandwidth of four-wave mixing in rb vapour, *Communications Physics* **1**, 84 (2018).
- [20] G. Kulkarni, L. Taneja, S. Aarav, and A. K. Jha, Angular schmidt spectrum of entangled photons: Derivation of an exact formula and experimental characterization for non-collinear phase matching, *Physical Review A* **97**, 063846 (2018).
- [21] A. Mair, A. Vaziri, G. Weihs, and A. Zeilinger, Entanglement of the orbital angular momentum states of photons, *Nature* **412**, 313 (2001).
- [22] K. Pang, C. Liu, G. Xie, Y. Ren, Z. Zhao, R. Zhang, Y. Cao, J. Zhao, H. Song, H. Song, *et al.*, Demonstration of a 10 mbit/s quantum communication link by encoding data on two laguerre–gaussian modes with different radial indices, *Optics Letters* **43**, 5639 (2018).
- [23] H. Larocque, D. Sagic, D. Mortimer, A. J. Taylor, R. Fickler, R. W. Boyd, M. R. Dennis, and E. Karimi, Reconstructing the topology of optical polarization knots, *Nature Physics* **14**, 1079 (2018).
- [24] J. Leach, M. R. Dennis, J. Courtial, and M. J. Padgett, Vortex knots in light, *New Journal of Physics* **7**, 55 (2005).
- [25] M. R. Dennis, R. P. King, B. Jack, K. O'holleran, and M. J. Padgett, Isolated optical vortex knots, *Nature Physics* **6**, 118 (2010).
- [26] M. Liscidini and J. Sipe, Stimulated emission tomography, *Physical review letters* **111**, 193602 (2013).
- [27] Y. Yang, P. Zhang, and X.-S. Ma, Stimulated emission tomography for entangled photon pairs with different detection spectral ranges, *JOSA B* **37**, 2071 (2020).
- [28] B. Fang, M. Liscidini, J. Sipe, and V. Lorenz, Multidimensional characterization of an entangled photon-pair source via stimulated emission tomography, *Optics express* **24**, 10013 (2016).
- [29] A. Keller, A. Z. Khoury, N. Fabre, M. Amanti, F. Baboux, S. Ducci, and P. Milman, Reconstructing the full modal structure of photonic states by stimulated-emission tomography in the low-gain regime, *Physical Review A* **106**, 063709 (2022).
- [30] Y. Xu, S. Tang, A. N. Black, and R. W. Boyd, Orthogonal spatial coding with stimulated parametric downconversion, *Optics Express* **31**, 42723 (2023).
- [31] S. P. Walborn, C. Monken, S. Pádua, and P. S. Ribeiro, Spatial correlations in parametric down-conversion, *Physics Reports* **495**, 87 (2010).
- [32] See Supplemental Material at URL-will-be-inserted-by-publisher for the data of the experiments.
- [33] Y. Miyamoto, D. Kawase, M. Takeda, K. Sasaki, and S. Takeuchi, Detection of superposition in the orbital angular momentum of photons without excess components and its application in the verification of non-classical correlation, *Journal of Optics* **13**, 064027 (2011).
- [34] A. Nicolas, L. Veissier, E. Giacobino, D. Maxein, and J. Laurat, Quantum state tomography of orbital angular momentum photonic qubits via a projection-based technique, *New Journal of Physics* **17**, 033037 (2015).
- [35] B. Baghdasaryan, F. Steinlechner, and S. Fritzsche, Justifying the thin-crystal approximation in spontaneous parametric down-conversion for collinear phase matching, *Phys. Rev. A* **103**, 063508 (2021).
- [36] T. Santiago-Cruz, A. Fedotova, V. Sultanov, M. A. Weissflog, D. Arslan, M. Younesi, T. Pertsch, I. Staude, F. Setzpfandt, and M. Chekhova, Photon pairs from resonant metasurfaces, *Nano letters* **21**, 4423 (2021).
- [37] G. Kulkarni, R. Sahu, O. S. Magaña-Loaiza, R. W. Boyd, and A. K. Jha, Single-shot measurement of the orbital-angular-momentum spectrum of light, *Nature communications* **8**, 1054 (2017).
- [38] G. Kulkarni, J. Rioux, B. Braverman, M. V. Chekhova, and R. W. Boyd, Classical model of spontaneous parametric down-conversion, *Physical Review Research* **4**, 033098 (2022).
- [39] B. Jack, P. Aursand, S. Franke-Arnold, D. G. Ireland, J. Leach, S. M. Barnett, and M. J. Padgett, Demonstration of the angular uncertainty principle for single photons, *Journal of Optics* **13**, 064017 (2011).
- [40] Y. Zhou, M. Mirhosseini, D. Fu, J. Zhao, S. M. H. Rafsanjani, A. E. Willner, and R. W. Boyd, Sorting photons by radial quantum number, *Physical review letters* **119**, 263602 (2017).
- [41] Y. Zhang, Multi-plane light conversion: a practical tutorial, *arXiv preprint arXiv:2304.11323* (2023).